Non-Enzymatic Polymerization into Long Linear RNA Templated by Liquid Crystal Self-Assembly

Marco Todisco[1], Tommaso P. Fraccia[1,2], Greg P. Smith[3], Andrea Corno[1], Lucas Bethge[4], Sven Klussmann[4], Elvezia M. Paraboschi[5], Rosanna Asselta[5,6], Diego Colombo[1], Giuliano Zanchetta[1], Noel A. Clark[3], Tommaso Bellini[1,*]

1 - Dipartimento di Biotecnologie Mediche e Medicina Traslazionale, Università di Milano, via Vanvitelli 32, 20129 Milano, Italy

2 - Dipartimento di Scienze Umane e Promozione della Qualità della Vita, Università San Raffaele di Roma, via di Val Cannuta, 247, I-00166 Roma (RM), Italy

3 - Department of Physics and Soft Materials Research Center, University of Colorado, Boulder, CO, 80309-0390

4 - NOXXON Pharma AG, 10589 Berlin, Germany

5- Department of Biomedical Sciences, Humanitas University, via Rita Levi Montalcini 4, I-20090 Pieve Emanuele (MI), Italy

6 - Humanitas Clinical and Research Center, via Alessandro Manzoni 56, I-20089 Rozzano (MI), Italy

*Address correspondence to tommaso.bellini@unimi.it

Self-synthesizing materials, in which supramolecular structuring enhances the formation of new molecules that participate to the process, represent an intriguing notion to account for the first appearance of biomolecules in an abiotic Earth. We present here a study of the abiotic formation of inter-chain phosphodiester bonds in solutions of short RNA oligomers in various states of supramolecular arrangement and their reaction kinetics. We found a spectrum of conditions in which RNA oligomers self-assemble and phase separate into highly concentrated ordered fluid liquid crystal (LC) microdomains. We show that such supramolecular state provides a template guiding their ligation into hundred-bases long chains. The quantitative analysis presented here demonstrates that nucleic acid LC boosts the rate of end-to-end ligation and suppresses the formation of the otherwise dominant cyclic oligomers. These results strengthen the concept of supramolecular ordering as an efficient pathway toward the emergence of the RNA World in the primordial Earth.

KEYWORDS self-assembly, liquid crystals, supramolecular chemistry, RNA World, origin of life, ligation, microreactors

The growing awareness of the relevance of supramolecular ordering on chemical reactivity is suggesting new routes for the emerging of patterns and structures.[1–4] Relevant examples are given by the self-synthesizing materials, in which self-assembly of amphiphilic molecules provides a template for covalent bond formation, which in turn promotes and stabilizes the supramolecular structures.[5,6] Indeed, it has been observed that supramolecular assembly can play a pivotal role in chemical reactions, directing the regioselectivity and boosting the reaction kinetics. Through this route, new symmetries and patterns may arise, reflecting more the mechanisms of molecular assembly than the reactivity of the isolated substrate. Because of this, it has been suggested that self-assembly-guided reactions could emerge as a rich strategy for the design of nanostructured materials and as a promising pathway to understand fundamental mysteries such as the origin of life.[1,6–11] In this last context, one of the main challenges is understanding the spontaneous formation of nucleic acid polymers from their monomeric constituents,[12,13] since it has to overcome several critical issues, such as: the extreme low reactivity of nucleotides,[14,15] the spontaneous tendency to form cyclical products contrasting the elongation of the polymers,[16,17] the high hydrolysis rate of phosphodiester bonds in aqueous environments[18] especially for RNA, and the competition of a variety of other potentially available reactive species, which would require a powerful selection mechanism.

In this study, we demonstrate and quantitatively characterize a non-enzymatic reaction pathway based on supramolecular assembly that favors the formation of long linear RNA chains by ligating short RNA oligomers. This work stems from a previous observation that the onset of liquid crystal ordering in solutions of DNA 12mers promotes their polymerization.[19] By a combination of different approaches, we demonstrate here the templating effect of the self-assembly of RNA oligomers, by which the geometry of the supramolecular aggregates favors intermolecular reactions over intramolecular reactions, while the local packing boosts the reaction rate. In this study, we considered shorter (6-base-long) and longer (12-base-long) RNA oligomers forming duplexes with terminal overhangs or blunt-ends, respectively, and we considered natural D-RNA and enantiomeric L-RNA.

Liquid crystal ordering as a general supramolecular motif of nucleic acids. The reversible but selective interaction among nucleic acid chains at the core of the processing of genetic information, relies on pairing and stacking interactions of nucleobases and on the good water solubility of the chains, granted by the ionized phosphate groups. These features confer to nucleic acids rather unique self-assembly properties, enabling the formation of extremely complex natural and artificial structures, such as the hierarchical structure of chromatin and the multi-strand constructs of DNA

nanotechnology.[20] In a series of papers,[21–26] we have shown that the same structural features and interactions lead, in aqueous solutions of short DNA oligomers at high concentration (c_{DNA} > 200mg/ml), to long-ranged supramolecular liquid crystal (LC) ordering afforded by hierarchical steps of self-assembly. LC ordering appears indeed as a rather general form of spontaneous ordering in DNA solutions and can be accompanied by the segregation of DNA LC domains when duplex-forming oligomers are mixed with unduplexed DNA strands, or with flexible polymers (*e.g.* PEG),[27] or with duplexes incapable to form linear columns.[23]

Liquid crystal as a step for the origin of life. The emergence of early life and DNA as the genetic polymer is widely thought to have proceeded through the so-called "RNA World", featuring RNA filaments playing the double role of carrying information and sustaining primordial metabolism.[28,29] Such catalytic RNA strands, the "ribozymes", first discovered by Cech and coworkers,[30] are chains having specific sequences and secondary structures. Tube-test evolution indicates that the minimum length of an RNA strand capable of providing the simplest enzymatic activity (cleavage of an RNA substrate) is of only 16 nt,[31] while more complex catalytic activities, such as the template-directed polymerization of NTPs on an external template, require much longer sequences, in the order of 150nt.[32] These are challenging lengths to be reached starting from mononucleotides or even from short oligomers, since their spontaneous formation is highly improbable. Indeed, the origin of the RNA World[33] is one of the main unsolved enigma of our understanding of nature.

In the search of a convincing "guiding hand", capable of selecting and ligating simple molecular groups into RNA strands,[8,34] various mechanisms have been proposed relying on templates and enhancers such as clay surfaces,[35,36] lipid assemblies[37–40] and pairing of nicked oligomers on a templating RNA strand.[41,42] The crucial search of a prebiotically plausible leaving group for phosphate condensation reaction has fostered the study of different compounds based on imidazole to overcome the low reactivity of polyphosphate.[43,44] The investigation of efficient methods to enhance linear polymerization over cyclization – a must to obtain long RNA strands – has highlighted the importance of base pairing and stacking interactions of building blocks[45] and the role of aromatic base-intercalating molecules.[16]

Based on the intimate connection between features that enable propagating genetic information, and those that promote LC ordering, we recently proposed[19,46] that the LC ordering of ultrashort nucleic acid oligomers could provide a positive feedback loop driving their abiotic ligation into longer oligomers. Indeed, in condensed LC phases the oligomers are stacked and organized into columns, each

being formed by a physically continuous but chemically discontinuous double helix in which the oligomer termini are held in close proximity. According to this scenario, the supramolecular assembly acts as a template guiding intermolecular ligation toward the formation of long linear chains when in the presence of appropriate reaction conditions. At the same time, the formation and stability of LCs is strongly dependent on the molecular shape anisotropy, since the presence of longer double helices lowers the concentration required for the onset of LC ordering. This establishes a positive feedback by which the ligation reaction guided by liquid crystals ordering promote their own self-assembly.

In previous experiments performed in solutions of 5'(OH) - 3'(p) DNA 12-base-long oligomers, we found that the onset of LC ordering markedly increased the inter-oligomer polymerization yield.[19]

On the basis of this seminal study we decided to explore the intimate nature of the templating effect of the liquid crystal ordering of nucleic acids in terms of reaction rates and products structure, as a non-peptidic example of self-synthesizing material. We focus here on RNA molecules, generally considered a more ancient nucleic acid than DNA. The extension of the LC properties from DNA to RNA is not trivial, since RNA has an A-form duplex helical structure, with paired bases tilted with respect to the helical axis,[47] a geometry of stacking that could affect the supramolecular structure.[48] While the conditions at which the prebiotic synthesis could have occurred are basically unknown, current scenarios are based on the notion of drying-wetting and heating-cooling cycles, possibly in the presence of thermal and chemical gradients such as those that can be found in inland hydrothermal springs[49] or in porous minerals surrounding oceanic hydrothermal vents.[50] The experiment we describe here are in conditions of mild temperature, and of molecular concentrations and ionic strengths naturally achieved in drying cycles, and thus in line with the current explorations in the research devoted to the origin of life.

RESULTS AND DISCUSSION

RNA oligomers. We studied two RNA oligomers of length 12 and 6:

i) 5'-pCGCGAAUUCGCG-3' (12BE), a self-complementary sequence forming terminal blunt-ends whose DNA analog we previously investigated.[21] 12BE used in this study is L-RNA, synthesized using L-ribose, and its structure is thus mirror symmetric with respect to natural RNA.[51] The use of L-RNA has the considerable advantage of being unaffected by the action of natural RNase, which has the potential of significantly affecting the quantitative analysis here proposed.

ii) 5'-pGAUCGC-3' (6SE), a partially self-complementary sequence. 6SE form 4-base-long paired duplexes with 2-base-long GC "adhesive" overhangs. 6SE in this study is D-RNA and is thus

potentially affected by RNase degradation. We indeed used enzymatic degradation as a tool to further characterize 6SE LC-promoted RNA ligation.

Both 12BE and 6SE terminate, on the 5' end, with a phosphate group that provides the starting point of the ligation reaction. We opted for the 5' terminus instead of the 3' end to make sure that no cyclization between 2' and 3' on the same sugar moiety could occur. With this choice, the ligation could lead to either 5'-2' or 5'-3' phosphodiester bonds. This depends on the regioselectivity in the non-enzymatic formation of phosphodiester bonds, which, in the case of inter-duplex ligation, is unknown. The ligation of nicked oligomers on a template strand has been found to be highly selective towards 5'-3' linkage,[52,53] despite the fact that 2'-hydroxyl group is more nucleophilic than 3'-hydroxyl group.[54]

Abiotic activator. Even if it's not considered a prebiotically plausible molecule, as proof of concept, we performed condensation reactions by using the water-soluble carbodiimide EDC (N-ethyl-N'-(dimethylaminopropyl) carbodiimide), which can react with terminal phosphate groups making them reactive toward nucleophiles, like primary amines[45] (yielding phosphoramidates), hydroxyl NA termini[55] (phosphodiesters) or water (hydrolysis). Surprising high yields (more than 90%) were previously observed in DNA LC,[19] which suggest a strong templating effect of this form of supramolecular ordering.

Phase behavior. RNA oligomers spontaneously order into LC phases. Fig. 1 illustrates typical textures observed in polarized optical microscopy showing coexistence of chiral nematic (N*) and columnar (COL) phases (panel a, showing a COL domain surrounded by N*) and COL phase (panels b and c, where the COL phase is recognizable from the characteristic fan-shaped domain). These phases appear at high RNA concentrations (c_{RNA} > 250mg/ml at room temperature) and in a broad interval of temperatures (T), as shown in the phase diagrams of 12BE (Fig. 1d) and 6SE (Fig. 1e). For both systems, the solutions display N* ordering (blue shading) and COL ordering at increasing c_{RNA} (red shading). Overall, the two phase diagrams are rather similar, indicating that the smaller axial ratio of 6SE duplexes – typically disfavoring LC ordering,[21] is compensated by their stronger overhang-mediated end-to-end coupling. The phase boundaries reported here for 12BE are not significantly dissimilar from those found for the analogous DNA molecule. These results suggest that the RNA inter-duplex stacking is at least as large as in the case of DNA.

To identify the best conditions for ligation experiments, we underwent a more detailed analysis of the phase behavior. First, we tested the effects of Mg^{2+}, which we found to stabilize the RNA LC phases.

This is shown by the dashed purple lines in the phase diagrams that mark the LC-isotropic phase boundary when 12BE and 6SE solutions are prepared with 60 mM $MgCl_2$. We then studied the phase behavior of mixtures of 12BE and PEG (MW 8000), employed as molecular crowding agent. We previously found that for sufficiently large PEG concentration, DNA/PEG solutions demix into coexisting DNA-rich and PEG-rich fluids.[19,27] We thus made an effort to determine the conditions under which the system phase separates adopting the morphology of RNA-rich microdomains surrounded by the PEG-rich isotropic phase. In this condition the system is effectively formed by microreactors where the reaction takes place, which are held by PEG osmotic pressure with no membrane or barrier for the diffusion of ions, EDC and waste products.

We thus carefully explored the phase behavior obtained by solubilizing a moderate amount of 12BE ($c_{RNA} \approx 37$ mg/ml) as a function of PEG concentration, as shown in Fig. 1f. The solutions are prepared in 60 mM $MgCl_2$ to take advantage of the stabilizing effect of Mg^{2+} ions. We find that for $c_{PEG} \leq 100$ mg/ml the solution remains homogeneous, while for $c_{PEG} \geq 150$ mg/ml RNA-rich microdomains start to appear. Depending on T, the RNA-rich domains are found either in isotropic (ISO) state (orange dots, orange shading) or as LC (green triangles, green shading). The two conditions are shown in the polarized microscopy pictures, where liquid-liquid (Fig. 1g) and liquid-LC (Fig. 1h) phase coexistence can be distinguished by the colors appearing in the birefringent LC domains as opposed to the dark, isotropic PEG-rich background. By a quantitative analysis of the phase diagram (described in the SI) we determined the limiting solubility of RNA in the PEG-rich phase to be $c_{RNA} \approx 13$ mg/ml, and the RNA concentration within the microdomains for two PEG concentrations: {$c_{PEG} = 150$ mg/ml, $c_{RNA} \approx 230$ mg/ml} and {$c_{PEG} = 200$ mg/ml, $c_{RNA} \approx 600$ mg/ml}. This analysis enabled us to pinpoint the conditions in which well-determined amount of RNA oligomers are effectively confined in membrane-less micro-reactors. We also found that an analogous phase separation and confinement effect can be obtained by mixing 12BE with single strand RNA (sequence 5'-CCUCAAAACUCC-3'), as described in the SI.

The phase diagram in Fig. 1f enables identifying T = 40°C as a convenient isothermal condition where to investigate the efficiency of EDC promoted ligation in mixtures of 12BE and PEG. At this T, upon increasing c_{PEG}, the system transitions from homogeneous mixture (where RNA is diluted, $c_{RNA} \approx 37$ mg/ml), to liquid-liquid coexistence (where RNA is concentrated but disordered, $c_{RNA} \approx 230$ mg/ml) to liquid-LC coexistence (where RNA is concentrated and ordered, $c_{RNA} \approx 600$ mg/ml).

A similar condition could not be found for 6SE/PEG mixtures where we find liquid-LC coexistence at room T (T = 25 °C) for $c_{PEG} \geq 100$ mg/ml, but no liquid-liquid coexistence at any T, since upon heating

the system transforms directly from liquid-LC coexistence to homogeneous (Fig. S17). We thus explored EDC promoted ligation in 6SE/PEG mixtures at room T.

Abiotic ligation in solutions of RNA oligomers. Fig. 2 summarizes the results of ligation experiments in 6SE/PEG ($c_{RNA} \approx 100$ mg/ml ≈ 50 mM) and in 12BE/PEG ($c_{RNA} \approx 37$ mg/ml ≈ 10 mM) mixtures with 60 mM $MgCl_2$, 0.01 M HEPES buffer pH 7.5, molar ratio EDC/RNA of 30, and various c_{PEG}. The energy source is provided by the water-soluble condensing agent EDC, through the reaction summarized in Fig. 3a. The ligation products have been evaluated by stopping the reaction at various time points (from 15min to 48h) by 20-fold dilution with 50 mM ethanolamine and by analyzing the mixture by 15% polyacrylamide gel electrophoresis in denaturing conditions, 7M urea, and staining with SYBR Gold (see SI). The phase separation and LC nucleation time is much faster than all reaction times here explored. The outcome of 48 hours reactions is shown in Fig. 2a for 12BE/PEG, each gel lane corresponding to different c_{PEG} and phases, as also described by the associated pictorial sketches. The presence of longer chains is enhanced by the phase separation (orange frame) and markedly boosted by the appearance of LC ordering (green frame).

Examples of profiles of the fluorescent intensity in the gels $I_F(x)$ are shown in Fig. 2c (black lines) for the ligation experiments with $c_{PEG} = 0$ mg/ml and $c_{PEG} = 250$ mg/ml, where the x coordinate along the lanes provides the product length associated with the bands. A reasonable estimate of the polymerization yield, defined as the fraction of newly formed phosphodiester bonds over the starting available 5' terminal phosphates, can be obtained by comparing the experimental cumulative I_F (colored dots) with the one predicted by a Flory model for simple polymerization (continuous line),[19,56] indicating that LC ordering leads to a markedly larger yield. Equivalently, the mean size of the products $\overline{n_b}$, plotted in Fig. 2d as a function of the PEG concentration shows that the increment associated to LC ordering is evident. According to this analysis in LC phase we obtain polymerization yields of 66%, 71% and 69% for c_{PEG} = 200 mg/ml, 250 mg/ml and 300 mg/ml respectively, corresponding to a fraction of more than 50% of the products being more than 5 times larger than the monomer ($n_b \geq 60$). This finding contrasts the moderate ligation yields found in the mixed solutions and in the liquid-liquid coexistence, where the average length of the products never exceeds twice and three times the monomer length, respectively.

Similar results are found for 6SE/PEG (Fig. 2b), where the enhancement of ligation efficiency brought about by phase separation and LC ordering is evident. In this case, though, the product mass distribution is not well described by the Flory model, due to a lower fluorescence emission of the

monomer. This limitation prevents us to assess the reaction yield *via* gel analysis. However, the low molecular weight of 6SE enabled us to perform Nuclear Magnetic Resonance (NMR) and unambiguously assign the signals in the ^{1}H and ^{13}C spectra. Particularly, ^{1}H NMR reveals broadening of the peaks in the 6SE sample treated with EDC (Fig. 3a), a well-known feature reflecting polymer formation.[57] ^{13}C NMR experiment allows the study of the anomeric carbons of the nucleotides sugars. As apparent in Fig. 3b, EDC treatment causes the disappearance of the signal assigned to the first nucleotide of the monomer (1' G1) and the appearance of a new signal assigned to the first nucleotide (1' G8) of the molecule bound to another oligo, thus offering an additional evidence of ligation. The quantitative comparison of the G8 peak with a reference peak (*i.e.* the peak at 88.5 ppm remains unchanged between unreacted and reacted sample) and with the background noise indicates that in the ligation reaction of 6SE occurring in LC, the fraction of 5'P termini involved in phosphodiester bonds is of the order of 90% (see Full NMR Spectra file and SI for more details).

In principle, LC-promoted RNA ligation could also influence the regioselectivity (5'-3' vs. 5'-2') of the newly produced phosphodiester bonds. The NMR analysis of 6SE ligation products (see SI) reveals no peak corresponding to 2'-5' phosphodiester bond formation, as expected for complementary strand templating,[52,53] making it hard to decouple a possible contribution of the supramolecular ordering. At the moment, our data do not enable assessing the role of LC-promoted RNA ligation alone in guiding the regioselectivity of the products, which could in principle be extracted by 12BE ligation products analysis.

Ligation reaction kinetics: dependence on supramolecular ordering. In the abiotic ligation reaction scheme exploited in this work (Fig. 4a) the energy source driving the reaction is provided by EDC, that can either hydrolyze into water (with a rate k_h), or activate the phosphate termini (k_1) producing an intermediate (Fig. 4a, red frame), which could in turn hydrolyze into EDU (N-ethyl-N'-(3-dimethylaminopropyl) urea) and a phosphate terminus (k_2), or produce a phosphodiester bond with the 3' or 2' hydroxyl terminus (k_L). Our data point to an enhancement of ligation efficiency linked to the transition to liquid crystalline state (Fig. 2), which could be due to a loss of entropy of activation thanks to the positional constraint provided by the LC-stabilized columnar stacking of duplexes that holds the duplex termini in continuous contact. Since this enhancement effect could in principle also originate from the higher RNA concentration of the LC phase, or even take place outside the LC domains, we performed an extended set of measurements aiming at quantifying the reaction rates, to clarify whether LC ordering can indeed be considered a templating milieu. The analysis outlined below and detailed in

the SI indicates that the effect of LC ordering can be described as an enhancement of k_L by at least 6 times.

In a first group of observations, we measured the evolution in time of the absorption spectra of solutions of either EDC only, or EDC with various concentrations of 5'phosphate ribose. This molecule, in which the phosphate moiety is analogous to the 5' termini of oligonucleotide chains, has been chosen to study the activation of the phosphate, because of its negligible absorbance in the UV range of interest (Fig. 4b). These measurements were performed in solutions of 60 mM $MgCl_2$, and HEPES buffer pH = 7.3, adjusted to match the pH measured in LC-forming PEG/EDC/RNA solutions. The measured spectra can all be perfectly fitted by a combination of the EDC and EDU spectra (Fig. 4d), with amplitudes that evolve in time as exponentials and sum up to a time-independent constant (Fig. 4e), as visually noticeable by the neat isosbestic point. No trace of the absorption spectrum of the activated phosphate could be observed, despite its chemical structure would suggest a detectable absorbance, an indication that the concentration of this group is negligible, in turn indicating a large k_2 value. By analyzing the data with a set of coupled linear kinetic equation describing the reaction steps in Fig. 4a, we could exploit this simplified condition to quantify the rates k_h and k_1 (see SI), while for k_2 only lower boundaries can be given.

To pinpoint the effects of LC ordering on ligation, we studied in depth the ligation reaction in the PEG/EDC/12BE mixture by starting from the simplest condition, *i.e.* at low PEG (c_{PEG} = 100 mg/ml), where the system remains in the mixed state. We examined the ligation products obtained in this condition as a function of the reaction time (blue squares in Fig. 4c) and fitted to the same set of coupled linear reaction equations. By keeping k_h and k_1 as determined above, the model predicts the yield to depend only on the ratio k_L/k_2. By fitting the data, we obtain a nicely approximating curve (blue line in Fig. 4c) and $k_L/k_2 \approx 100$ (SI), indicating that the activated terminus is more reactive with the ribose OH at 2' or 3' position than with water.

At higher PEG concentration, where the system phase separates, the reaction becomes more complex since it could take place simultaneously in the two coexisting phases. This condition can still be modeled by a larger set of coupled linear equations (see SI), whose parameters include the relative volumes filled by the two phases and the RNA concentrations in both phases. Being diffusion of reagents an essential ingredient of the process, we made sure that the condensed phase was fluid and that EDC and EDU could diffuse in and out the domains. This was done by FRAP (Fluorescence Recovery After Photobleaching) measurements, which indicate that the equilibration time of molecules of the size of EDC and EDU takes place in a time much shorter than the reaction time so that reaction-

induced local EDC depletion can be neglected (see SI). We assume k_h and k_2, rates of reaction with water molecules, to be the same as in the mixed condition, since hydration always remains significant. Conversely, k_1 and k_L, might be, in the RNA-rich phase, significantly different than in the mixed state because of two concurring effects. First, the solubility of EDC in the RNA-rich solutions might be much smaller than in the PEG-rich phase, as suggested by the strong partitioning observed for fluorescent dopants of analogous molecular size (see SI). Moreover, the viscosity of the RNA-rich phase markedly grows with RNA concentration, as indicated by FRAP measurements. Since reaction rates are typically inversely proportional to viscosity[58] and viscosity grows more than linearly with RNA concentration (see SI), we expect k_1 and k_L to be decreased at least proportionally to the c_{RNA}: $k_1' = (F/c_{RNA})\, k_1$; $k_L' = (F/c_{RNA})\, k_L$, where F is proportionality coefficient. Ligation kinetics measured in liquid-liquid coexistence (c_{PEG} = 150 mg/ml, orange circles in Fig. 4c), is well approximated by the model with the choice F = 30 mM (orange line).

When we apply the same procedure with the same choice of rates k_h, k_1', k_2, k_L', to model the ligation kinetics in liquid-LC coexistence (green triangles in Fig. 4c), the model strongly underestimates the observed yield (dashed green line). To match the data we need to increase k_L of at least 6 times, a choice that leads to the continuous green line in Fig. 4c. In other words, we find that the rate of inter-strand ligation in LC is enhanced over what expected in an identical system that had no LC ordering by 6 time – possibly much more – indicating that the LC ordering is indeed promoting ligation, confirming the templating effect of this supramolecular self-assembly. We emphasize that the 6 increment is a lower estimate, since our FRAP experiments indicate that viscosity increases much more than proportionally to concentration as the LC ordering appears.

Having a tool to evaluate the EDC-promoted ligation in phase separated PEG/EDC/RNA solutions, we can split the observed yield into the contributions from the two coexisting phases (Fig. 2d, half dots). The model with the parameters determined as above indicates that the largest majority of the longer strands are indeed produced by the ligation reaction in the LC phase. The total yield, evaluated by gel electrophoresis is effectively lowered by the inefficient reaction in the PEG-rich, RNA-poor phase that fills most of the volume (see the determination of concentrations in RNA-PEG separate phases in SI).

Ligation products: dependence on supramolecular ordering. By holding duplexes in a fluid but ordered matrix, LC ordering not only promotes the formation of chemical bonds between the contacting termini, but also inhibits intramolecular ligation. The molecular packing within the LC phase stabilizes the duplexes and holds them stacked into linear aggregates thus disfavoring the

contacts between the termini within each duplex. Circular structures are instead expected to be a favorite outcome of the ligation reaction of duplexes in isotropic phases, where the transient melting of the terminal bases and their reaction can easily occur. This notion is supported by two distinct approaches described here: selective enzymatic digestion of 6SE ligation products and 2D-PAGE of 12BE products, which, being L-RNA, cannot be enzymatically probed. This conclusion is further supported by NMR data, as discussed below.

In PEG/EDC/12BE mixtures, reaction products obtained in disordered solutions (Fig. 2a, blue and orange frames), contain a larger variety of smaller oligomers than reaction products in the LC phase (green frame). This is the case of the product leading to the PAGE band found in between the linear 24mer and 36mer and marked in Fig. 2a by a red arrow, which becomes almost undetectable in LC reactions. To explore the difference between these bands, we have run 2D-PAGE experiments, an older technique to characterize mixtures of RNA molecules that are not resolved in a simple 1D-PAGE experiment. This technique, which takes advantage of the fact that the migration velocity of oligomers of distinct topology depends differently on the concentration of the gel,[59] has been used to characterize complex tRNA mixtures and solutions of RNA polymers.[60] By using 2D-PAGE, we find a markedly different behavior of the red arrow-marked band with respect to the one closest to it, indicating that they have distinct topologies (see SI). The simplest topological difference between 24mers is linear vs. circular. Indeed, circular ssRNAs are known to have a slower electrophoretic mobility as compared to the linear molecules of equal length,[61] in line with the position of this extra band of different mobility.

Production of circular oligomers also appears as the reason behind the lower apparent ligation yield in 6SE PAGE. The two-base long overhangs make the formation of phosphodiester bonds between the 5' and 3' (or 2') termini of unbound 6SE duplexes much easier than in the blunt-ended structure of 12BE. The formation of a significant fraction of circular oligomers in PEG/EDC/6SE mixtures is demonstrated by the combination of two observations. NMR ^{13}C signals from the anomeric carbons indicate that virtually all 6SE 5' terminal phosphates are involved in phosphodiester bonds (see SI). This evidence demonstrates that the ligation yield is much larger than the one determined by product length distribution, a condition which is found if a significant fraction of the oligomers is circular. Indeed, PAGE analysis reveals a number of bands larger than the expected multiples of 6SE (Fig. 2b, green frame). We thus performed enzymatic degradation of the reaction products of 6SE by SVP (Snake Venom Phosphodiesterase I), an enzyme known to degrade nucleic acid molecules with an efficiency larger for linear than for circular strands.[62–64] We dispersed 0.1mU of SVP in the reaction products of PEG/EDC/6SE with c_{PEG} = 250 mg/ml and compared the effects of enzymatic degradation

at different times, as shown in Fig. 5. Quite clearly, the SVP action on the various products is uneven, as apparent in the section zoomed in panel b and analyzed in panel c. Two of the bands (red squares and green triangles) are almost completely degraded after 5 minutes, while the intensity of the third (blue dots) decreases in the same time of only about 20%. This result enables the identification of the former as linear and the latter as circular products, thus justifying the large number of bands. It also indicates that they alternate in the gel, which is consistent with the attribution resulting from the 2D PAGE gels in 12BE reaction products (see SI): linear strands have larger electrophoretic mobility than circular chains of equal mass.

All this evidence supports the notion that the molecular template provided by LC ordering is a crucial factor in guiding polymerization toward long polymers, since in its absence intramolecular cyclization is the dominant reaction pathway.

CONCLUSION

In this work, we have demonstrated the templating effect of LC ordering in solutions of RNA oligomers. Our results provide an example of self-synthesizing material, in which self-assembly promotes the formation of products that in turn stabilize the assembly. At the same time, our results strengthen the notion that LC ordering may have had a role in favoring the first emergence of RNA polymers as a product of ligation between short oligomers.

Our study has been organized in steps.

1. We have found that solutions of RNA oligomers develop LC ordering in a wide range of chain lengths, concentrations and temperatures. We thoroughly investigated the phase diagrams, identifying the conditions more amenable to a ligation reaction. Specifically, we found that RNA oligomers can be concentrated and segregated using PEG as a molecular crowding agent and that the presence of Mg^{2+} ions has a stabilizing effect on RNA LC phases, significantly promoting phase separation in RNA-PEG mixtures.
2. We thus studied the ligation reaction in mixtures in which RNA oligomers are organized in fluid micro-domains, either liquid or LC, coexisting with a liquid phase rich in PEG that acts as a reservoir for EDC, a carbodiimide agent that activates the terminal phosphates, and as a sink for waste. We have found that, as LC ordering appears, the length of the reaction products markedly increases, to the point that almost 50% of the resulting chains is more than 5 times longer than the starting oligomers. The mean average length of the products increases from 24 bases (twice the

initial 12mer) to 72 bases (6 times) when the reaction is carried in isotropic and LC phase respectively.

3. We have thus focused on understanding which, among the various steps involved in the reaction, is the one that promotes the enhanced ligation and why. By combining the study of the reaction kinetics in various conditions, of the partitioning of the solutes in the coexisting phases, of the viscosity of the RNA solutions, we managed to disentangle the various contributions in the ligation reactions and show that the appearance of LC ordering markedly enhances the last step of the reaction, *i.e.* the formation of phosphodiester bonds between the activated 5' terminal phosphate and the 3' (or 2') OH terminus. This result is a proof that the effect of LC ordering is indeed a consequence of the template provided by the collective molecular ordering. The geometrical constraint exerted on each duplex lowers the entropic cost of covalent bonding, thus speeding up the reaction. Our observations suggest an analogy between LC templating and enzyme-promoted chemical ligation between the termini of nucleic acid chains. Indeed, the action of ligases relies on the combination of various factors, including (i) the use of molecular energy sources, such as ATP, to produce a reactive intermediate (ii) the positional constraint on the two termini following their binding to the ligase, (iii) the reduction of the free energy of the transition state provided by the loss of entropy of the reactants and thanks to the electro-chemical environment in the enzyme active site. The LC-promoted abiotic ligation reaction pathway bears relevant analogies to the working scheme of ligase enzymes: (i) the energy source is here provided by EDC, whose reaction produces a reactive intermediate (ii) kept in close proximity to a reactive terminus by the LC milieu, (iii) thus reducing the entropy of activation of the transition state in the reaction step leading to the formation of a new phosphodiester bond.

4. We have found LC ordering strongly disfavors the formation of cyclic products, which instead appear to be the favored outcome when reaction between duplex termini takes place in a liquid phase. Indeed, the formation of circular products is a potential dead-end of abiotic polymerization and thus a fatal obstacle in the spontaneous emergence of long RNA polymers on the early Earth. This is a recognized problem for the spontaneous polymerization of unstructured fluids. Previous studies have proposed the presence of inter-base intercalating molecules as a possible mechanism disfavoring cyclization.[16]

Our results indicate that both templating effect and polymerization in linear chains are promoted by supramolecular ordering with no need of external guiding constraints such as intercalators, lipids or mineral surfaces. The efficacy of LC ordering in promoting the formation of linear RNA polymers is

the result of two combined factors: molecular order and fluidity. The onset of uniaxial LC ordering brings about a symmetry breaking that is reflected at the microscopic level as a molecular field stabilizing linear aggregates and suppressing supramolecular clusters having alternative geometries, such as circular or disordered aggregates. Fluidity enables the diffusion – albeit slowed down by the increased viscosity – of reactant and waste molecules and the circulation of the duplexes.

To which extent the conditions here considered are compatible with the primordial Earth is of course a matter of speculation. The presence of short oligomers could have been promoted by lipid assisted polymerization of single nucleotides.[37,39,40] The concentration necessary for LC templating could have been achieved either in inland hydrothermal water ponds fed by hot springs, by hydration-dehydration cycles,[12,49] or in oceanic hydrothermal pores by accumulation of RNA molecules driven by thermophoresis.[50,65] Both sites are characterized by temperature variations compatible with those explored in this work.[49,50] Ionic strength and Mg^{2+} concentration used in our experiments are also in line with the expected composition of prebiotic water. In modern oceans, the Mg^{2+} concentration is about 54 mM, while in the anoxic water of primordial oceans it is estimated to be around 10 mM[66,67] and in the sweet water of inland thermal springs is of the order of few millimolar.[49,66] PEG and EDC are instead not prebiotically plausible molecules. Indeed, we have used them not because they represent a realistic model, but for their effectiveness in generating conditions that could have been produced in many other ways. PEG has been used in this work as a molecular crowder. In general, crowding can result from dehydration or from phase separation. PEG induces and enables easy control of aqueous two-phase systems, which have been considered as a model systems for coacervates, which are thought to have played a crucial role in selecting and clustering molecules in prebiotic environments.[68–71] Other molecular species, such as polysaccharides, cationic oligopeptides and low molecular weight polycations (as spermine and spermidine), have also been found to induce coacervation,[72,73] providing a set of more prebiotically plausible alternatives to PEG. Analogously, while EDC has been chosen for its fast reactivity to enable demonstrating the intimate connection between LC ordering and linear polymerization, other phosphate activating molecules, such as cyanogen bromide[74] and N-cyanoimidazole,[75] could represent prebiotically plausible alternatives to EDC

Overall, our experiments provide a proof of concept of LC templating: indeed, should there have been an “RNA World” on the primordial Earth, our results suggest that it could have been preceded by a “LC World”, whose appearance requires much shorter chains, in which supramolecular ordering provided molecular selection and geometrical template for the polymerization of long linear RNA chains.

METHODS

Solid phase RNA synthesis & purification. RNA-oligonucleotides were assembled on an Äkta10 Oligopilot synthesizer (Amersham Biosciences; GE Healthcare, Freiburg, D) in a 1.2 mL fixed volume column using standard RNA phosphoramidites. Phosphoramidites were purchased from Proligo (Hambug,Germany, D-RNAphosphoramidites) and ChemGenes (Wilmington,USA, L-RNA phosphoramidites). Base-loaded solid support was purchased from Prime Synthesis (Aston, PA, USA). Synthesis was started from base-loaded CPG, pore size 600 Å. For coupling (12 min per cycle), 0.6 M ethylthiotetrazole (Azide Chemical Co., Ltd, Anzhen, Wuxi, CN) in acetonitrile, and 6 equivalents of the respective 0.2 M phosphoramidite solution in acetonitrile were used.

A capping-oxidation-capping cycle was applied. Standard solvents and reagents for oligonucleotide synthesis were purchased from Biosolve (Valkenswaard, NL), Proligo (Hamburg, D), VWR (Karlsruhe, D) or Sigma Aldrich (Taufkirchen, D). Cleavage and deprotection were achieved according to Wincott *et al.*[76] with minor alterations. In detail, upon completion of the automated synthesis, the CPG-bound oligonucleotide (10-15 μmol) was briefly dried and transferred into a glass bottle. 20mL of aq. $MeNH_2$ (40%) were added, and the suspension was gently agitated at room temperature. After 90 min the slurry was filtered, and the residual CPG washed several times with aq. EtOH (50%). The combined filtrates were concentrated and lyophilized. For the removal of the 2'TBDMS groups, the dry crude product was dissolved in 1.5mL DMSO followed by 0.75mL NEt3 and 1.0mL NEt3·3HF. This mixture was gently agitated at 65°C for 2h. After cooling to room temperature, 20mL n-BuOH was added and the resulting precipitate was collected and washed with acetone. Crude oligonucleotides were purified by ion exchange HPLC (IEX) followed by Salt removal size exclusion chromatography (NAP10, GE-Healthcare, Freiburg, Germany). The final products were dried by lyophilization and stored at -20°C until further use. Purity and identity were confirmed by IEX- and RP-HPLC and LC-MS.

Microscope cells preparation. Lyophilized 5'-phosphate RNA was resuspended in milliQ water at a concentration of 50 mg/ml and stored at -20°C to slow down spontaneous hydrolysis. Samples for microscope observations (microscope cells) were prepared placing one or multiple drops (0.5-1 μl) of the RNA solution on a glass slide, waiting for them to dry and resuspending them in an appropriate volume of solutions based on milliQ water, $MgCl_2$ and buffered PEG8k to reach the final desired concentration directly on the slide.

To observe these sample in standard bright field, polarized light and fluorescence microscopy, a second glass slide was placed on the top of the solution and kept at a controlled distance using 10-20 μm silica spacer rods. The LC domains explored in this study are thus much larger than both molecular and aggregate sizes. The cells were sealed with fluorinated oil to keep the sample concentration stable over long periods of time at high temperature.

C_{RNA} vs temperature phase diagram measurement. The measurement of RNA concentration in microscope cells was performed through microscope-based interferometry.[21] One or multiple drops of concentrated RNA (initial concentration = 50 mg/ml) were placed on a high-refractive index glass (n = 1.62), sandwiched and slowly concentrated through evaporation at room temperature before being sealed with fluorinated oil at different times to produce an array of different final concentrations. The liquid crystalline solutions prepared in this way were equilibrated through multiple thermal cycles, taking note of the different phases exhibited as a function of temperature, and finally brought to isotropic phase, where the spectrum of the light reflected in the RNA solution was acquired. The multiple reflection fringes due to the interference from the parallel glass plates were systematically measured in various spots within the isotropic RNA solution and in the fluorinated oil (of known refractive index) present at the edges of the cell. This set of data enabled determining the exact thickness of the cell and the refractive index of the RNA solution, and thus the RNA concentration c_{RNA} through a calibration curve ($n = n_0+dn/dc \cdot c$), with n_0 the refractive index of the solution at zero RNA concentration and $dn/dc = 0.136$ cm^3/g).

1D PAGE. 2 μg of reaction product in 5 μl were mixed with 3 μl of loading solution (30% glycerol) and 10 μl of formamide and loaded in a 7 M urea denaturing 15% polyacrylamide gel (size 20 x 20 x 0.1 cm^3). Gels were run in a Protean apparatus (Biorad) in TBE buffer at 250V for approximately 2.5 hours. SYBR Gold 1x in TBE buffer was used as staining for 5 min and gel images were acquired in .tif format using a Gel Doc EZ Imager (Biorad).

2D PAGE. A single lane was excised from the 1D gel and stacked on top of a second 7 M urea denaturing 20% polyacrylamide gel (size 20 x 20 x 0.1 cm^3). The two gels were sealed together using fresh 20% polyacrylamide gel. The second dimension was run at 300V for approximately 4 hours. Staining and image acquisition were done as previously described.

Analysis of polymerization yield. Lane profiles of the acquired gel images were estimated using MacBiophotonics ImageJ software. Assuming linearity between the fluorescence intensity of the peaks and the RNA concentration, it is possible to measure the product in each gel band. The cumulative fluorescence signal of the different length product is fitted with Flory Model equation for a simple polymerization[56] $h(p,x) = 1-p^x-x\cdot p^x+x\cdot p^{(1+x)}$, describing the products length distribution of a system where monomers have the same probability p to bound and p is independent from polymer length. See SI for a more detailed description. Each experimental condition has been repeated three times in distinct microscope cells and the measured yields have been found to be consistent.

pH determination. The pH of RNA/PEG8k/$MgCl_2$/EDC mixtures was measured using an Orion™ 9810BN Micro pH Electrode. The pH determined in this way is equal to 7.3. Unless otherwise stated all the spectrophotometric measurements have been performed using an excess of HEPES pH 7.3 buffer to match the mixtures pH.

Determination of concentrations in PEG-separated phases. To evaluate the concentration of RNA in the PEG-rich phase, we measured the relative volumes filled by the RNA-rich phase as a function of c_{RNA} (T = 25 °C, 60 mM $MgCl_2$) in c_{PEG} = 150 mg/ml and c_{PEG} = 200 mg/ml mixtures. As c_{RNA} concentration is increased, the volume fraction occupied by birefringent domains increases linearly, and the RNA concentration in the domains can be obtained from the proportionality coefficient. See SI for a more detailed description.

FRAP-based measurement of samples viscosity. We used Sodium Fluorescein as fluorophore to probe the viscosity of the RNA and RNA-PEG mixtures, due to its hydrodynamic radius (r = 0.45 nm) being comparable to the one of EDC. Bleaching was induced focusing a Xenon Lamp source over an area of 80μm-400μm of radius on the sample with a high magnification objective (20x or 50x). Recovery was recorded using a low magnification objective (4x or 10x) and neutral filters to reduce bleaching during the acquisition. Data analysis was performed according to Soumpasis model.[77] See SI for more details.

Determination of k_h and k_1 using UV-spectrophotometry. k_h can be readily determined by monitoring the time evolution of the EDC absorbance spectrum and the corresponding appearance and growth of the absorption spectrum of EDU as shown in Fig. S11, left-hand panel. Normalized profiles

were fitted using a simple exponential decay e^{-kt} (right-hand panels). We obtain $k_h \approx 0.033$ h^{-1}. To measure k_1 we monitored the decay of EDC in mixtures with 5'phosphate ribose (P for simplicity), adding various amounts of P and fitting the decay of the amplitude of the EDC spectrum with $c \cdot e^{(t(-[P]\cdot k1-kh))}$, where c is the initial EDC concentration, [P] is the concentration of 5'phosphate ribose, and k_h is held as previously determined. See SI for more details.

Modeling the ligation reaction. The reaction described in Fig. 4 of the main text can be modeled by a set of coupled linear reactions (see SI Eqs S11). These equations, combined with the conservation constraints between species, can be solved to obtain the expected evolution of all species. Since no analytical solution is available, we solved them numerically using ODE45 function in MATLAB, searching for the best k_2 to k_L ratio ($R = k_2 / k_L$) to fit our experimental data (implemented *via* the *fminsolve* function) for product formation obtained from PAGE gels as described above. The value of the parameter R that best reproduces our experimental data in the mixed state is $R \approx 1.11\ 10^{-2}$. See SI for more details. Eqs. S11 are conceived for a homogeneous solution. When the system phase separates, the reaction takes place simultaneously in the two phases. The set of coupled equations can be modified to take into account this different condition introducing the parameters F_{in} and F_{out} as the volume fractions of the two phases (see SI Eqs S12) and incorporating into the system the larger viscosity in the RNA-rich phases. See SI for more details.

NMR characterization of ligation products. We performed high resolution nuclear magnetic resonance (NMR) spectroscopy on two 6SE samples: a 6SE stock solution (6SE) and a 6SE sample which underwent 48h ligation reaction in LC phase (6SE-LIG), c_{PEG} = 200 mg/ml and EDC 30X. ^{1}H NMR analyses were performed at 500 MHz with a Bruker FT-NMR AVANCE™ DRX500 spectrometer using a 5-mm z-PFG (pulsed field gradient) broadband reverse probe at 298 K or 343K, and ^{13}C NMR spectra were collected at 125.76 MHz. The signals were unambiguously assigned by 2D COSY, NOESY (only 298 K) and HSQC experiments.[78,79] ^{1}H NMR chemical shifts are reported as δ (ppm) relative to residual HDO fixed at 4.705 and 4.716 ppm for spectra recorded at 298 K and 343 K, respectively. See SI for more details.

Enzymatic Digestion of 6SE. 6SE ligation with EDC were treated with SVP, Snake Venom Phosphodiesterase I from *Crotalus adamanteus* (Sigma Aldrich). The lyophilized enzyme was resuspended in 4 ml of reaction buffer (Tris-HCl 10mM pH 8.8, NaCl 25mM, $MgCl_2$ 10mM) and 1μl

was added to a 9 μl solution of the ligated RNA diluted in reaction buffer. Final RNA concentration in digestion reaction is ≈ 0.1 – 0.2 mg/ml, final enzyme activity is ≈ 0.01 U/ml. The reaction was run at room temperature and stopped after 5', 10', 30' and 60' adding 2 μl of 55mM EDTA pH 8 to the mixtures and immediately storing them at -20°C. See SI for more details.

Authors Contributions: M.T., T.P.F., G.P.S., G.Z., N.A.C., T.B. conceived the experiments; L.B. and S.K. synthesized and purified the oligomers; M.T., T.P.F., A.C. measured phase diagrams and defined the ligation conditions; M.T., T.P.F. performed ligation experiments and enzymatic digestion; M.T., E.M.P., R.A. performed PAGE; M.T. performed UV absorbance and FRAP experiments; M.T., T.B. analyzed the data; T.P.F., D.C. performed the NMR measurements; M.T., T.P.F., G.Z., N.A.C., T.B. wrote the manuscript.

Acknowledgments: This research was supported in part by the NSF Biomaterials Program under Grant DMR-1611272 and DMR-1420736, by NSF Materials Research. We wish to thank T. Carzaniga, F. Giavazzi and S. Sattin for useful discussions. M.T. acknowledges the support of the Invernizzi Fundation.

Supporting Information Available: Full NMR spectra, additional figures (S1-S17) and detailed description of 2D PAGE gels, enzymatic digestion of 6SE, analysis of polymerization yield, characterization of reaction mixtures, determination of reaction rates, NMR characterization of ligation products. This material is available free of charge *via* the Internet at http://pubs.acs.org.

REFERENCES

(1) Bissette, A. J.; Fletcher, S. P. Mechanisms of Autocatalysis. *Angew. Chemie - Int. Ed.* **2013**, *52*, 12800–12826.

(2) Li, J.; Carnall, J. M. A.; Stuart, M. C. A.; Otto, S. Hydrogel Formation upon Photoinduced Covalent Capture of Macrocycle Stacks from Dynamic Combinatorial Libraries. *Angew. Chemie - Int. Ed.* **2011**, *50*, 8384–8386.

(3) Omosun, T. O.; Hsieh, M. C.; Childers, W. S.; Das, D.; Mehta, A. K.; Anthony, N. R.; Pan, T.; Grover, M. A.; Berland, K. M.; Lynn, D. G. Catalytic Diversity in Self-Propagating Peptide Assemblies. *Nat. Chem.* **2017**, *9*, 805–809.

(4) Makhlynets, O. V.; Gosavi, P. M.; Korendovych, I. V. Short Self-Assembling Peptides Are Able to Bind to Copper and Activate Oxygen. *Angew. Chemie - Int. Ed.* **2016**, *55*, 9017–9020.

(5) Rubinov, B.; Wagner, N.; Matmor, M.; Regev, O.; Ashkenasy, N.; Ashkenasy, G. Transient Fibril Structures Facilitating Nonenzymatic Self-Replication. *ACS Nano* **2012**, *6*, 7893–7901.

(6) Rout, S. K.; Friedmann, M. P.; Riek, R.; Greenwald, J. A Prebiotic Template-Directed Peptide Synthesis Based on Amyloids. *Nat. Commun.* **2018**, *9, 234*.

(7) Ashkenasy, G.; Hermans, T. M.; Otto, S.; Taylor, A. F. Systems Chemistry. *Chem. Soc. Rev.* **2017**, *46*, 2543–2554.

(8) Budin, I.; Szostak, J. W. Expanding Roles for Diverse Physical Phenomena During the Origin of Life. *Annu. Rev. Biophys.* **2010**, *39*, 245–263.

(9) Cafferty, B. J.; Gállego, I.; Chen, M. C.; Farley, K. I.; Eritja, R.; Hud, N. V. Efficient Self-Assembly in Water of Long Noncovalent Polymers by Nucleobase Analogues. *J. Am. Chem. Soc.* **2013**, *135*, 2447–2450.

(10) Davis, J. G.; Gierszal, K. P.; Wang, P.; Ben-Amotz, D. Water Structural Transformation at Molecular Hydrophobic Interfaces. *Nature* **2012**, *491*, 582–585.

(11) Szostak, J. W. The Narrow Road to the Deep Past: In Search of the Chemistry of the Origin of Life. *Angew. Chemie - Int. Ed.* **2017**, *56*, 11037–11043.

(12) Pearce, B. K. D.; Pudritz, R. E.; Semenov, D. A.; Henning, T. K. Origin of the RNA World: The Fate of Nucleobases in Warm Little Ponds. *Proc. Natl. Acad. Sci. U. S. A.* **2017**, *114*, 11327-11332.

(13) Powner, M. W.; Gerland, B.; Sutherland, J. D. Synthesis of Activated Pyrimidine Ribonucleotides in Prebiotically Plausible Conditions. *Nature* **2009**, *459*, 239–242.

(14) Mamajanov, I.; Macdonald, P. J.; Ying, J.; Duncanson, D. M.; Dowdy, G. R.; Walker, C. A.; Engelhart, A. E.; Fernández, F. M.; Grover, M. A.; Hud, N. V.; Schork, F.J. Ester Formation and Hydrolysis during Wet-Dry Cycles: Generation of Far-from-Equilibrium Polymers in a Model Prebiotic Reaction. *Macromolecules* **2014**, *47*, 1334–1343.

(15) Toppozini, L.; Dies, H.; Deamer, D. W.; Rheinstädter, M. C. Adenosine Monophosphate Forms Ordered Arrays in Multilamellar Lipid Matrices: Insights into Assembly of Nucleic Acid for Primitive Life. *PLoS One* **2013**, *8*, 1–8.

(16) Horowitz, E. D.; Engelhart, A. E.; Chen, M. C.; Quarles, K. a; Smith, M. W.; Lynn, D. G.; Hud, N. V. Intercalation as a Means to Suppress Cyclization and Promote Polymerization of Base-Pairing Oligonucleotides in a Prebiotic World. *Proc. Natl. Acad. Sci. U. S. A.* **2010**, *107*, 5288–5293.

(17) Kuruvilla, E.; Schuster, G. B.; Hud, N. V. Enhanced Nonenzymatic Ligation of Homopurine Miniduplexes: Support for Greater Base Stacking in a Pre-RNA World. *ChemBioChem* **2013**, *14*, 45–48.

(18) Benner, S. A.; Kim, H. J.; Carrigan, M. A. Asphalt, Water, and the Prebiotic Synthesis of Ribose, Ribonucleosides, and RNA. *Acc. Chem. Res.* **2012**, *45*, 2025–2034.

(19) Fraccia, T. P.; Smith, G. P.; Zanchetta, G.; Paraboschi, E.; Yi, Y.; Walba, D. M.; Dieci, G.; Clark, N. A.; Bellini, T. Abiotic Ligation of DNA Oligomers Templated by Their Liquid Crystal Ordering. *Nat. Commun.* **2015**, *6*, 6424.

(20) Jones, M. R.; Seeman, N. C.; Mirkin, C. A. Programmable Materials and the Nature of the DNA Bond. *Science* **2015**, *347*, 1260901–1260901.

(21) Nakata, M.; Zanchetta, G.; Chapman, B. D.; Jones, C. D.; Cross, J. O.; Pindak, R.; Bellini, T.; Clark, N. A. End-to-End Stacking and Liquid Crystal Condensation of 6 to 20 Base Pair DNA Duplexes. *Science* **2007**, *318*, 1276–1279.

(22) Zanchetta, G.; Nakata, M.; Buscaglia, M.; Clark, N. A.; Bellini, T. Liquid Crystal Ordering of DNA and RNA Oligomers with Partially Overlapping Sequences. *J. Phys. Condens. Matter* **2008**, *20*, 494214–494219.

(23) Bellini, T.; Zanchetta, G.; Fraccia, T. P.; Cerbino, R.; Tsai, E.; Smith, G. P. Liquid Crystal Self-Assembly of Random- Sequence DNA Oligomers. *Proc. Natl. Acad. Sci. U. S. A.* **2012**, *109*, 1–6.

(24) Fraccia, T. P.; Smith, G. P.; Bethge, L.; Zanchetta, G.; Nava, G.; Klussmann, S.; Clark, N. A.; Bellini, T. Liquid Crystal Ordering and Isotropic Gelation in Solutions of Four-Base-Long DNA Oligomers.

ACS Nano **2016**, *10*, 8508−8516.

(25) Smith, G. P.; Fraccia, T. P.; Todisco, M.; Zanchetta, G.; Zhu, C.; Hayden, E.; Bellini, T.; Clark, N. A. Backbone-Free Duplex-Stacked Monomer Nucleic Acids Exhibiting Watson – Crick Selectivity. *Proc. Natl. Acad. Sci. U. S. A.* **2018**, *115*, E7658–E7664.

(26) Fraccia, T. P.; Smith, G. P.; Clark, N. A.; Bellini, T. Liquid Crystal Ordering of Four-Base-Long DNA Oligomers with Both G–C and A–T Pairing. *Crystals* **2018**, *8,* 494214-494219.

(27) Zanchetta, G.; Nakata, M.; Buscaglia, M.; Bellini, T.; Clark, N. A. Phase Separation and Liquid Crystallization of Complementary Sequences in Mixtures of NanoDNA Oligomers. *Proc. Natl. Acad. Sci. U. S. A.* **2008**, *105*, 1111–1117.

(28) Gilbert, W. The RNA World. *Nature* **1986**, *319*, 618.

(29) Joyce, G. F. The Antiquity of RNA-Based Evolution. *Nature* **2002**, *418*, 214–221.

(30) Kruger, K.; Grabowski, P. J.; Zaug, A. J.; Sands, J.; Gottschling, D. E.; Cech, T. R. Self-Splicing RNA: Autoexcision and Autocyclization of the Ribosomal RNA Intervening Sequence of Tetrahymena. *Cell* **1982**, *31*, 147–157.

(31) Scott, W. G.; Finch, J. T.; Klug, A. The Crystal Structure of an AII-RNA hammerhead Ribozyme: A Proposed Mechanism for RNA Catalytic Cleavage. *Cell* **1995**, *81*, 991–1002.

(32) Johnston, W. K.; Unrau, P. J.; Lawrence, M. S.; Glasner, M. E.; Bartel, D. P. RNA-Catalyzed RNA Polymerization: Accurate and General RNA-Templated Primer Extension. *Science* **2001**, *292*, 1319–1325.

(33) Robertson, M. P.; Joyce, G. F. The Origins of the RNA World. *Cold Spring Harb. Perspect. Biol.* **2012**, *4*, a003608.

(34) De Duve, C. *Singularities - Landmarks on the Pathways of Life*; Cambridge University Press, 2005.

(35) Miyakawa, S.; Ferris, J. P. Sequence- and Regioselectivity in the Montmorillonite-Catalyzed Synthesis of RNA. *J. Am. Chem. Soc.* **2003**, *125*, 8202–8208.

(36) Huang, W.; Ferris, J. P. One-Step, Regioselective Synthesis of up to 50-Mers of RNA Oligomers by Montmorillonite Catalysis. *J. Am. Chem. Soc.* **2006**, *128*, 8914–8919.

(37) Rajamani, S.; Vlassov, A.; Benner, S.; Coombs, A.; Olasagasti, F.; Deamer, D. Lipid-Assisted Synthesis of RNA-like Polymers from Mononucleotides. *Orig. Life Evol. Biosph.* **2008**, *38*, 57–74.

(38) Mansy, S. S.; Schrum, J. P.; Krishnamurthy, M.; Tobé, S.; Treco, D. a; Szostak, J. W. Template-

Directed Synthesis of a Genetic Polymer in a Model Protocell. *Nature* **2008**, *454*, 122–125.

(39) Deguzman, V.; Vercoutere, W.; Shenasa, H.; Deamer, D. Generation of Oligonucleotides Under Hydrothermal Conditions by Non-Enzymatic Polymerization. *J. Mol. Evol.* **2014**, *78*, 251–262.

(40) Mungi, C. V; Rajamani, S. Characterization of RNA-Like Oligomers from Lipid-Assisted Nonenzymatic Synthesis: Implications for Origin of Informational Molecules on Early Earth. *Life* **2015**, *5*, 65–84.

(41) Von Kiedrowski, G. A Self-Replicating Hexadeoxynucleotide. *Angew. Chemie Int. Ed. English* **1986**, *25*, 932–935.

(42) Zielinski, W. S.; Orgel, L. E. Autocatalytic Synthesis of a Tetranucleotide Analogue. *Nature* **1987**, *327*, 346–347.

(43) Inoue, T.; Orgel, L. E. Substituent Control of the Poly (C)-Directed Oligomerization of Guanosine 5'-Phosphoroimidazolid. *J. Am. Chem. Soc.* **1981**, *103*, 7666–7667.

(44) Schrum, J. P.; Ricardo, A.; Krishnamurthy, M.; Blain, J. C.; Szostak, J. W. Efficient and Rapid Template-Directed Nucleic Acid Copying Using 2'-Amino-2',3'-Dideoxyribonucleoside-5'-Phosphorimidazolide Monomers. *J. Am. Chem. Soc.* **2009**, *131*, 14560–14570.

(45) Taran, O.; Thoennessen, O.; Achilles, K.; Von Kiedrowski, G. Synthesis of Information-Carrying Polymers of Mixed Sequences from Double Stranded Short Deoxynucleotides. *J. Syst. Chem.* **2010**, *1*, 9–24.

(46) Fraccia, T. P.; Zanchetta, G.; Rimoldi, V.; Clark, N. a.; Bellini, T. Evidence of Liquid Crystal–Assisted Abiotic Ligation of Nucleic Acids. *Orig. Life Evol. Biosph.* **2015**, *45*, 51–68.

(47) Calladine, C. R.; Drew, H. R.; Luisi, B. F.; Travers, A. A.; Calladine, C. R.; Drew, H. R.; Luisi, B. F.; Travers, A. A. Chapter 3 – Different Kinds of Double Helix. In *Understanding DNA*; 2004; pp 39–63.

(48) Zanchetta, G.; Bellini, T.; Nakata, M.; Clark, N. A. Physical Polymerization and Liquid Crystallization of RNA Oligomers. *J. Am. Chem. Soc.* **2008**, *130*, 12864–12865.

(49) Damer, B.; Deamer, D. Coupled Phases and Combinatorial Selection in Fluctuating Hydrothermal Pools: A Scenario to Guide Experimental Approaches to the Origin of Cellular Life. *Life* **2015**, *5*, 872–887.

(50) Baaske, P.; Weinert, F. M.; Duhr, S.; Lemke, K. H.; Russell, M. J.; Braun, D. Extreme Accumulation of Nucleotides in Simulated Hydrothermal Pore Systems. *Proc. Natl. Acad. Sci. U.*

S. A. **2007**, *104*, 9346–9351.

(51) Rossi, M.; Zanchetta, G.; Klussmann, S.; Clark, N. a.; Bellini, T. Propagation of Chirality in Mixtures of Natural and Enantiomeric Dna Oligomers. *Phys. Rev. Lett.* **2013**, *110*, 107801.

(52) Rohatgi, R.; Bartel, D. P.; Szostak, J. W. Nonenzymatic , Template-Directed Ligation of Oligoribonucleotides Is Highly Regioselective for the Formation of 3 ′ - 5 ′ Phosphodiester Bonds. *J. Am. Chem. Soc.* **1996**, *118*, 3340–3344.

(53) Sawai, H.; Wada, M.; Kouda, T.; Ozaki, A. N. Nonenzymatic Ligation of Short-Chained 2'-5'- or 3'-5'-Linked Oligoribonucleotides on 2'-5'- or 3'-5'-Linked Complementary Templates. *ChemBioChem* **2006**, *7*, 605–611.

(54) Lohrmann, R.; Orgel, L. E. Preferential Formation of (2'-5')-Linked Internucleotide Bonds in Non-Enzymatic Reactions. *Tetrahedron* **1978**, *34*, 853–855.

(55) Sokolova, N. I.; Ashirbekova, D. T.; Dolinnaya, N. G.; Shabarova, Z. A. Chemical Reactions within DNA Duplexes. Cyanogen Bromide as an Effective Oligodeoxyribonucleotide Coupling Agent. *FEBS Lett.* **1988**, *232*, 153–155.

(56) Flory, J. Molecular Size Distribution in Linear Condensation Polymers. *J. Am. Chem. Soc.* **1936**, *1*, 1877–1885.

(57) Voit, B.; Haag, R.; Appelhans, D.; Welzel, P. B. Chapter 4.1.1 – Structural Characterization. In *Bio- and Multifunctional Polymer Architectures: Principles, Synthetic Methods, and Applications*; John Wiley & Sons, 2016; pp 116

(58) Grabarek, Z.; Gergely, J. Zero-Length Crosslinking Procedure with the Use of Active Esters ☆. *Anal. Biochem.* **1990**, *185*, 131–135.

(59) Nowacka, M.; Jackowiak, P.; Rybarczyk, A.; Magacz, T.; Strozycki, P. M.; Barciszewski, J.; Figlerowicz, M. 2D-PAGE as an Effective Method of RNA Degradome Analysis. *Mol. Biol. Rep.* **2012**, *39*, 139–146.

(60) Fradin, A.; Gruhl, H.; Feldmann, H. Mapping of Yeast TRNAs by Two-Dimensional Electrophoresis on Polyacrylamide Gels. *FEBS Lett.* **1975**, *50*, 185–189.

(61) Hassall, J.; MacDonald, P.; Cordero, T.; Rostain, W.; Jaramillo, A. Design and Characterization of Topological Small RNAs. In *RNA Scaffolds. Methods in Molecular Biology*; 2015; pp 149–167.

(62) Zaphiropoulos, P. G. Circular RNAs from Transcripts of the Rat Cytochrome P450 2C24 Gene: Correlation with Exon Skipping. *Proc. Natl. Acad. Sci. U. S. A.* **1996**, *93*, 6536–6541.

(63) Gao, H.; Yang, M.; Patel, R.; Cook, A. F. Circularization of Oligonucleotides by Disulfide Bridge Formation. *Nucleic Acids Res.* **1995**, *23*, 2025–2029.

(64) Kowalski, D. A Procedure for the Quantitation of Relaxed Closed Circular DNA in the Presence of Superhelical DNA: An Improved Fluorometric Assay for Nicking-Closing Enzyme. *Anal. Biochem.* **1979**, *93*, 346–354.

(65) Mast, C. B.; Schink, S.; Gerland, U.; Braun, D. Escalation of Polymerization in a Thermal Gradient. *Proc. Natl. Acad. Sci. U. S. A.* **2013**, *110*, 8030–8035.

(66) Mulkidjanian, A. Y.; Bychkov, A. Y.; Dibrova, D. V.; Galperin, M. Y.; Koonin, E. V. Origin of First Cells at Terrestrial, Anoxic Geothermal Fields. *Proc. Natl. Acad. Sci.* **2012**, *109*, E821–E830.

(67) Holm, N. G. The Significance of Mg in Prebiotic Geochemistry. *Geobiology* **2012**, *10*, 269–279.

(68) Jia, T. Z.; Hentrich, C.; Szostak, J. W. Rapid RNA Exchange in Aqueous Two-Phase System and Coacervate Droplets. *Orig. Life Evol. Biosph.* **2014**, *44*, 1–12.

(69) Keating, C. D. Aqueous Phase Separation as a Possible Route to Compartmentalization of Biological Molecules. *Acc. Chem. Res.* **2012**, *45*, 2114–2124.

(70) Strulson, C. A.; Molden, R. C.; Keating, C. D.; Bevilacqua, P. C. RNA Catalysis through Compartmentalization. *Nat. Chem.* **2012**, *4*, 941.

(71) Lazcano, A. Historical Development of Origins Research. *Cold Spring Harb Perspect Biol* **2010**, *2*, a002089.

(72) Poudyal, R. R.; Pir Cakmak, F.; Keating, C. D.; Bevilacqua, P. C. Physical Principles and Extant Biology Reveal Roles for RNA-Containing Membraneless Compartments in Origins of Life Chemistry. *Biochemistry* **2018**, *57*, 2509–2519.

(73) Matthew, H. W.; Salley, S. O.; Peterson, W. D.; Klein, M. D. Complex Coacervate Microcapsules for Mammalian Cell Culture and Artificial Organ Development. *Biotechnol. Prog.* **1993**, *9*, 510–519.

(74) Dolinnaya, N. G.; Sokolova, N. I.; Ashirbekova, D. T.; Shabarova, Z. a. The Use of BrCN for Assembling Modified DNA Duplexes and DNA-RNA Hybrids; Comparison with Water-Soluble Carbodiimide. *Nucleic Acids Res.* **1991**, *19*, 3067–3072.

(75) Mariani, A.; Sutherland, J. D. Non-Enzymatic RNA Backbone Proofreading through Energy-Dissipative Recycling. *Angew. Chemie - Int. Ed.* **2017**, *56*, 6563–6566.

(76) Wincott, F.; Direnzo, A.; Shaffer, C.; Grimm, S.; Tracz, D.; Workman, C.; Sweedler, D.; Gonzalez,

C.; Scaringe, S.; Usman, N. Synthesis, Deprotection, Analysis and Purification of RNA and Ribosomes. *Nucleic Acids Res.* **1995**, *23*, 2677–2684.

(77) Soumpasis, D. M. Theoretical Analysis of Fluorescence Photobleaching Recovery Experiments. *Biophys. J.* **1983**, *41*, 95–97.

(78) Parella, T. Pulse Program Catalogue : Experiments. *Pulse Progr. Cat.* **2006**, 1–249.

(79) Kessler, H.; Gehrke, M.; Griesinger, C. Two-Dimensional NMR Spectroscopy: Background and Overview of the Experiments. *Angew. Chem., Int. Ed. Engl.* **1988**, *27*, 490–536.

TABLE OF CONTENT GRAPHIC

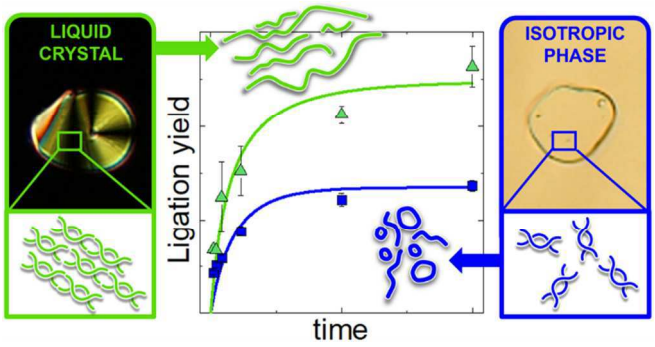

FIGURES CAPTIONS

Figure 1. Supramolecular liquid crystal ordering in aqueous solutions of RNA oligomers. (a, b, c) Pictures by polarized optical microscopy of liquid crystalline phases in 6mer 6SE: nematic/columnar coexistence (a) and columnar phases (b: c_{RNA} = 250 mg/ml, c: c_{RNA} = 350 mg/ml). Size bar shown in (a) is shared by (b) and (c). (d,e) Concentration (c_{RNA}) – temperature (T) phase diagrams of the RNA 12mer 12BE (d) and 6mer 6SE (e), whose duplex structures and self-assembly are sketched. Blue triangles and shading: chiral nematic phase (N*). Red dots and shading: columnar phase (COL). Black squares: isotropic phase (ISO). Empty dots: ISO-LC coexistence. Pink dashed line marks where the N* phase boundary is found when 60 mM Mg^{2+} is added to the solution. (f) PEG8k concentration (c_{PEG}) – T phase diagram for 10mM 12BE, 60 mM $MgCl_2$, yielding homogenous phase (blue squares and shading), liquid-liquid coexistence (orange dots and shading, and orange-framed microscope picture and sketch, panel g), liquid-LC coexistence (green triangles and shading, and green-framed polarized microscope pictures and sketch, panel h).

Figure 2. Ligation reaction in mixtures of RNA/PEG8k/$MgCl_2$/EDC. (a,b) Denaturing 15% PAGE of ligation products after 48 hours of reaction of 12BE at T=40 °C (a) and 6SE at T=25 °C (b) for various PEG8k content (c_{PEG}). Blue, orange, green frames and sketches indicate the mixed state, liquid-liquid coexistence and liquid-LC coexistence, respectively, in which reactions are performed. Lengths expressed as number of bases (n_b) are marked on the right-hand side of the PAGE gel pictures. The red arrow marks a double band discussed in the main text. (c,d) analysis of the reaction products for 12BE. (c) Fluorescence intensity (IF) profiles of the c_{PEG}=0 mg/ml and c_{PEG}=250 mg/ml lanes (black line) plotted vs n_b. Integrated IF (symbols) and their best fit to the Flory simple polymerization model (colored lines). (d) Average n_b of the reaction products vs. c_{PEG} (symbols and color code refer to the phase in which reactions are performed). For c_{PEG}=150 mg/ml and c_{PEG}=200 mg/ml the average n_b has been separated into the contributions from the two coexisting (RNA-rich and PEG-rich) phases.

Figure 3. NMR study of 6SE ligation in LC state. (a) Comparison of the aromatic bases protons region of ^{1}H NMR spectra of 6SE (top panel) and 6SE-LIG at 343K (bottom panel). Reacted samples show broadening of the peaks, giving a first clue for the formation of polymers in solution. (b) Comparison of ^{13}C NMR spectra of 6SE (top panel) and 6SE-LIG at 343K (bottom panel). The peak at 87.4 ppm (1' G1), corresponding to the anomeric carbon of the first G nucleotide of the monomer, disappears upon EDC treatment, while a peak at 87.8 ppm (1' G8) appears. This second peak is assigned to the anomeric carbon of the first G nucleotide belonging to a molecule preceded by a bound oligo, thus demonstrating ligation. Full NMR spectra are reported in the supporting material.

Figure 4. Ligation reaction kinetics. (a) Reaction steps and definition of the reaction rates. The red frame identifies the activated intermediate. Parameters shaded in yellow and green are determined as described in panels (b, d, e) and (c), respectively. (b) Example of k_1 measurement through UV-spectra acquisition over time for a diluted EDC + 5'phosphate ribose (P) mixture. Arrows indicate the evolution over time of the spectra, that show an isosbestic point. (d) Decomposition of the measured spectra as linear superposition of the EDC and EDU spectra. The relative amount of the two species is plot over time as shown in (e) and fit to determine k_1 and k_h. (c) 12BE polymerization yield vs time in 10mM RNA/PEG8k/60mM $MgCl_2$/300mM EDC in mixed solutions (c_{PEG}=100 mg/ml, blue squares), liquid-liquid coexistence (c_{PEG}=150 mg/ml, orange dots), liquid-LC coexistence (c_{PEG}=200 mg/ml, green triangles) at T=40°C. Continuous lines are the best fit obtained by modeling the reaction with a set of coupled linear equation. Fit to the mixed state (blue line) and to the liquid-liquid coexistence (orange line) enable determining all kinetic parameters. Dashed green line: prediction of the yield vs.

time for the liquid-LC coexistence by this choice of parameters. Continuous green line: prediction by the linear kinetic model when k_L is increased by 6 times.

Figure 5. Discrimination of 6SE linear vs. circular ligation products by SVP digestion. (a) Denaturing 20% PAGE of 6SE reaction products in liquid-LC coexistence (c_{PEG}=250 mg/ml) treated with Snake Venom Phosphodiesterase I (SVP). The digestion reaction has been stopped at different times (5', 10', 30', 60') to point out bands more efficiently digested. Gel contrast has been enhanced for a better visualization. (b) highlight of bands associated with lower weight products and (c) plot of relative intensities of the bands over time. Continuous lines are guides for the eye. An alternate pattern of easily and hardly digestible products emerges in the PAGE band sequence.

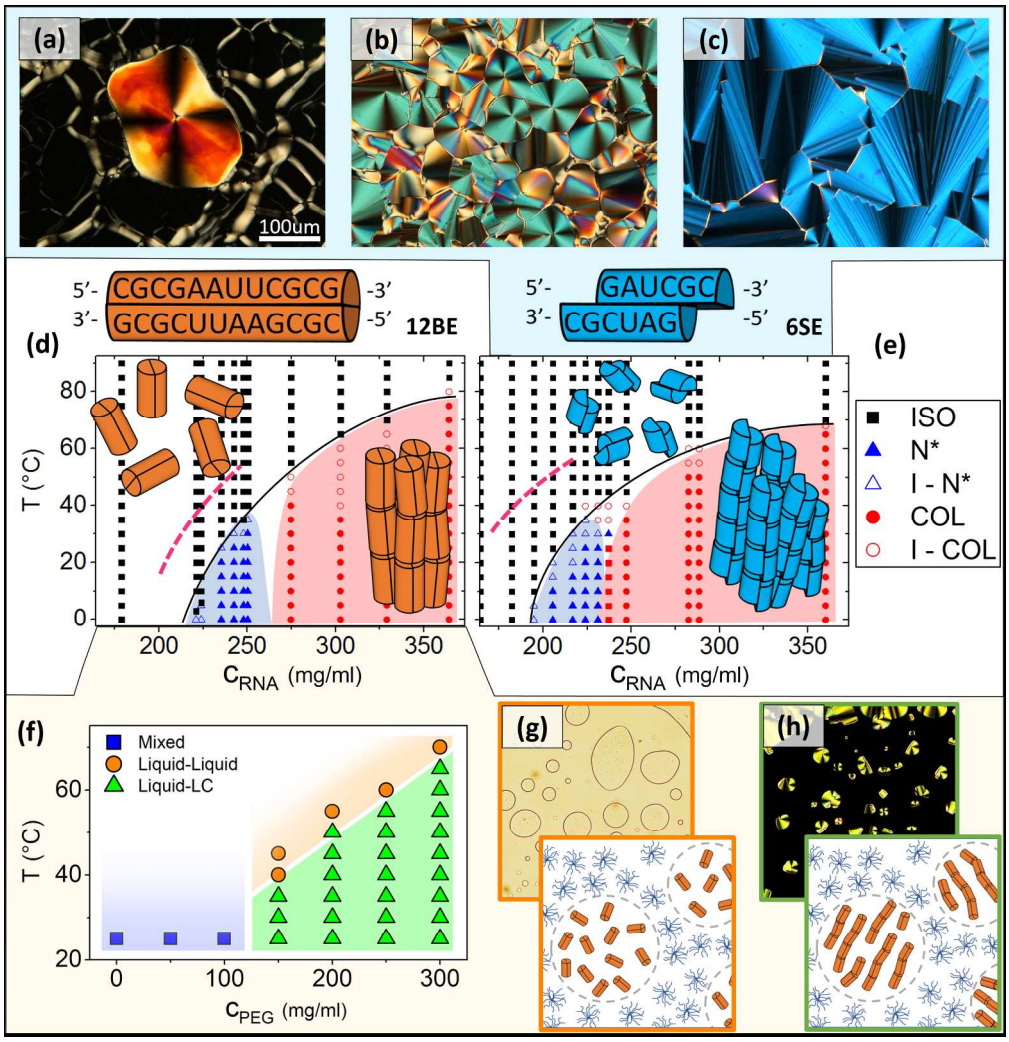

Figure 1. Supramolecular liquid crystal ordering in aqueous solutions of RNA oligomers. (a, b, c) Pictures by polarized optical microscopy of liquid crystalline phases in 6mer 6SE: nematic/columnar coexistence (a) and columnar phases (b: c_{RNA} = 250 mg/ml, c: c_{RNA} = 350 mg/ml). Size bar shown in (a) is shared by (b) and (c). (d,e) Concentration (c_{RNA}) – temperature (T) phase diagrams of the RNA 12mer 12BE (d) and 6mer 6SE (e), whose duplex structures and self-assembly are sketched. Blue triangles and shading: chiral nematic phase (N*). Red dots and shading: columnar phase (COL). Black squares: isotropic phase (ISO). Empty dots: ISO-LC coexistence. Pink dashed line marks where the N* phase boundary is found when 60 mM Mg^{2+} is added to the solution. (f) PEG8k concentration (c_{PEG}) – T phase diagram for 10mM 12BE, 60 mM $MgCl_2$, yielding homogenous phase (blue squares and shading), liquid-liquid coexistence (orange dots and shading, and orange-framed microscope picture and sketch, panel g), liquid-LC coexistence (green triangles and shading, and green-framed polarized microscope pictures and sketch, panel h).

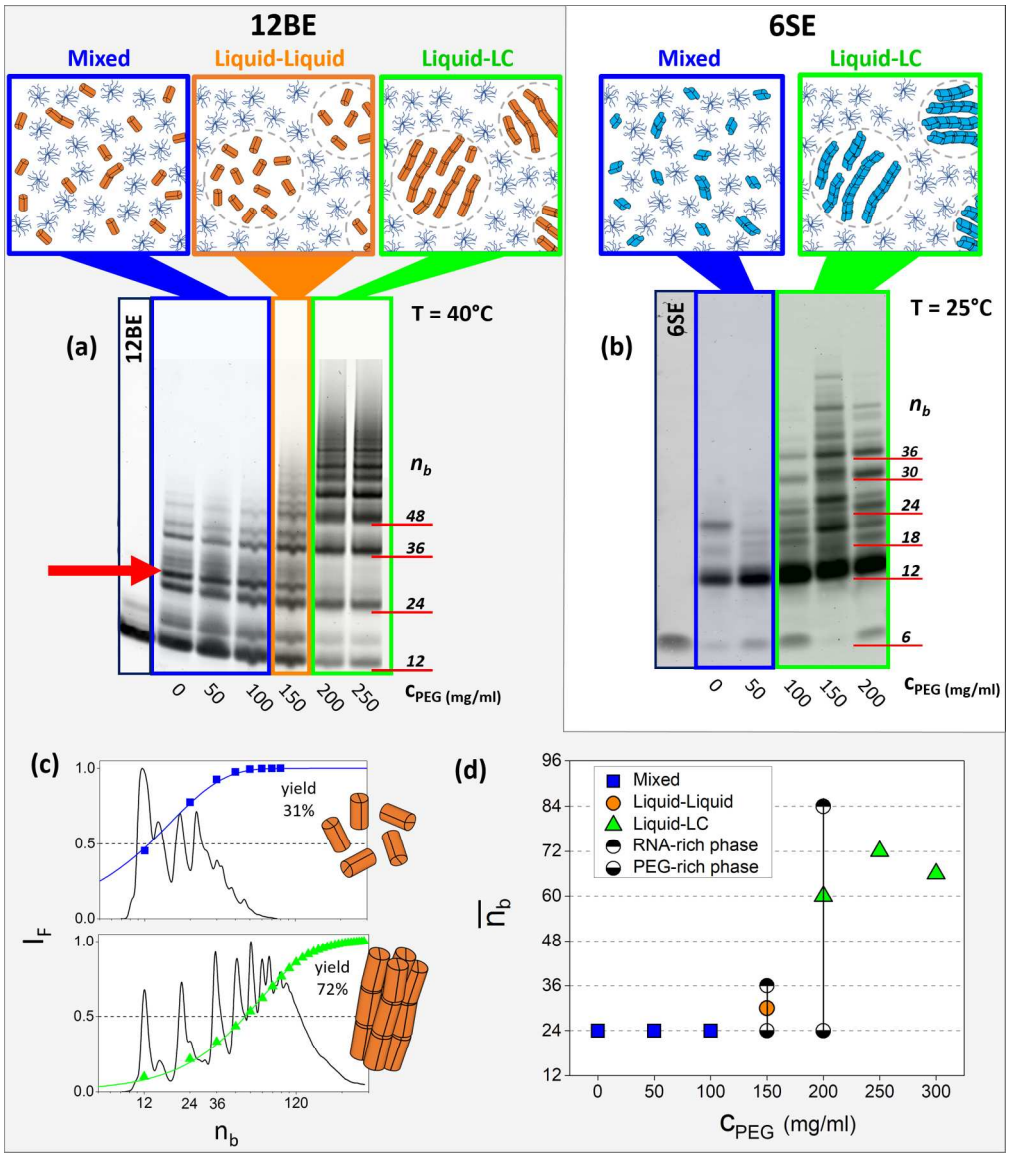

Figure 2. Ligation reaction in mixtures of RNA/PEG8k/$MgCl_2$/EDC. (a,b) Denaturing 15% PAGE of ligation products after 48 hours of reaction of 12BE at T=40 °C (a) and 6SE at T=25 °C (b) for various PEG8k content (c_{PEG}). Blue, orange, green frames and sketches indicate the mixed state, liquid-liquid coexistence and liquid-LC coexistence, respectively, in which reactions are performed. Lengths expressed as number of bases (n_b) are marked on the right-hand side of the PAGE gel pictures. The red arrow marks a double band discussed in the main text. (c,d) analysis of the reaction products for 12BE. (c) Fluorescence intensity (IF) profiles of the c_{PEG}=0 mg/ml and c_{PEG}=250 mg/ml lanes (black line) plotted vs n_b. Integrated IF (symbols) and their best fit to the Flory simple polymerization model (colored lines). (d) Average n_b of the reaction products vs. c_{PEG} (symbols and color code refer to the phase in which reactions are performed). For c_{PEG}=150 mg/ml and c_{PEG}=200 mg/ml the average n_b has been separated into the contributions from the two coexisting (RNA-rich and PEG-rich) phases.

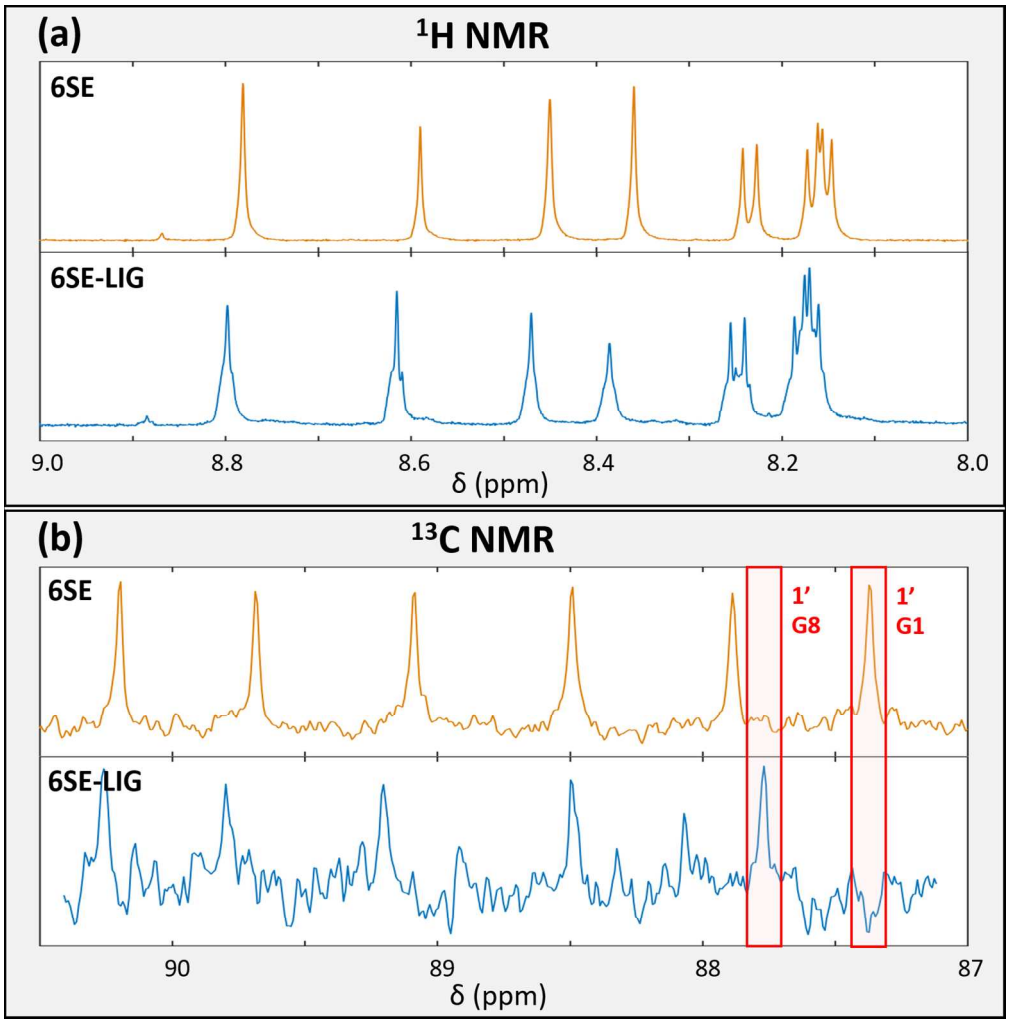

Figure 3. NMR study of 6SE ligation in LC state. (a) Comparison of the aromatic bases protons region of ^{1}H NMR spectra of 6SE (top panel) and 6SE-LIG at 343K (bottom panel). Reacted samples show broadening of the peaks, giving a first clue for the formation of polymers in solution. (b) Comparison of ^{13}C NMR spectra of 6SE (top panel) and 6SE-LIG at 343K (bottom panel). The peak at 87.4 ppm (1' G1), corresponding to the anomeric carbon of the first G nucleotide of the monomer, disappears upon EDC treatment, while a peak at 87.8 ppm (1' G8) appears. This second peak is assigned to the anomeric carbon of the first G nucleotide belonging to a molecule preceded by a bound oligo, thus demonstrating ligation. Full NMR spectra are reported in the supporting material.

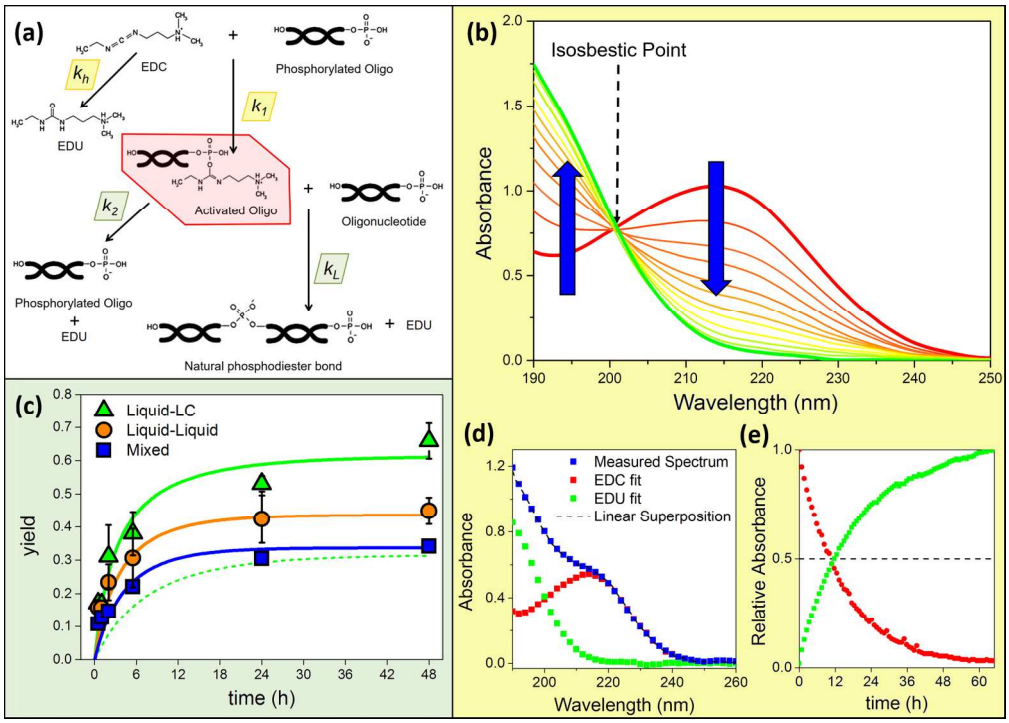

Figure 4. Ligation reaction kinetics. (a) Reaction steps and definition of the reaction rates. The red frame identifies the activated intermediate. Parameters shaded in yellow and green are determined as described in panels (b, d, e) and (c), respectively. (b) Example of k_1 measurement through UV-spectra acquisition over time for a diluted EDC + 5'phosphate ribose (P) mixture. Arrows indicate the evolution over time of the spectra, that show an isosbestic point. (d) Decomposition of the measured spectra as linear superposition of the EDC and EDU spectra. The relative amount of the two species is plot over time as shown in (e) and fit to determine k_1 and k_h. (c) 12BE polymerization yield vs time in 10mM RNA/PEG8k/60mM $MgCl_2$/300mM EDC in mixed solutions (c_{PEG}=100 mg/ml, blue squares), liquid-liquid coexistence (c_{PEG}=150 mg/ml, orange dots), liquid-LC coexistence (c_{PEG}=200 mg/ml, green triangles) at T=40°C. Continuous lines are the best fit obtained by modeling the reaction with a set of coupled linear equation. Fit to the mixed state (blue line) and to the liquid-liquid coexistence (orange line) enable determining all kinetic parameters. Dashed green line: prediction of the yield vs. time for the liquid-LC coexistence by this choice of parameters. Continuous green line: prediction by the linear kinetic model when k_L is increased by 6 times.

365x260mm (150 x 150 DPI)

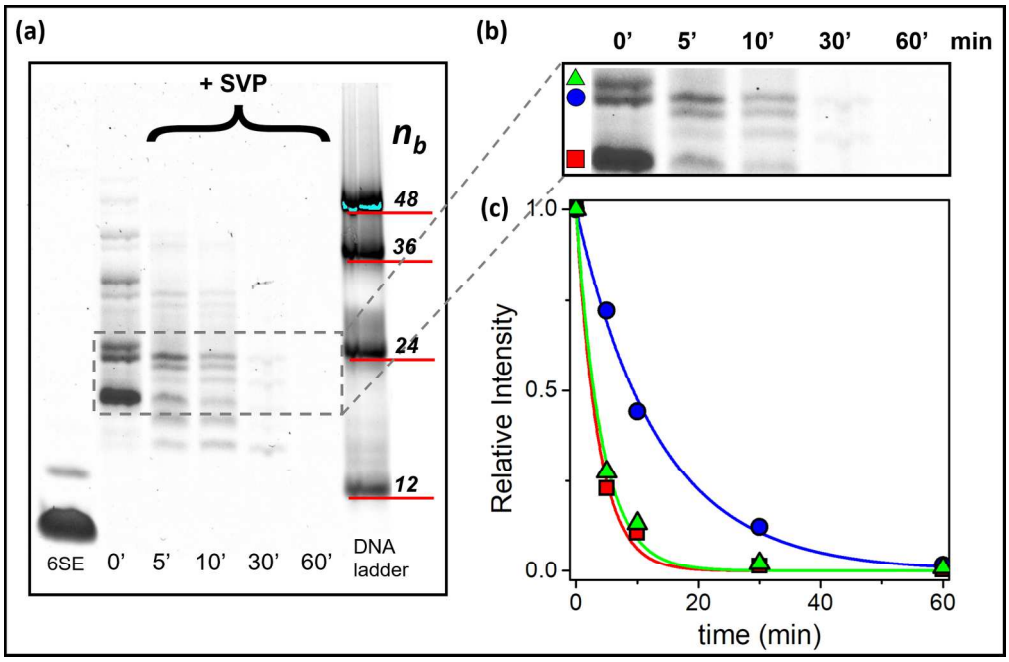

Figure 5. Discrimination of 6SE linear vs. circular ligation products by SVP digestion. (a) Denaturing 20% PAGE of 6SE reaction products in liquid-LC coexistence (c_{PEG}=250 mg/ml) treated with Snake Venom Phosphodiesterase I (SVP). The digestion reaction has been stopped at different times (5', 10', 30', 60') to point out bands more efficiently digested. Gel contrast has been enhanced for a better visualization. (b) highlight of bands associated with lower weight products and (c) plot of relative intensities of the bands over time. Continuous lines are guides for the eye. An alternate pattern of easily and hardly digestible products emerges in the PAGE band sequence.